

# Distinguishable-particle Glassy Crystal: the simplest molecular model of glass

Leo S.I. Lam<sup>1,\*</sup>, Gautham Gopinath<sup>2,3,\*</sup>, Zichen Zhao<sup>2,4,\*</sup>, Shuling Wang<sup>5,2</sup>, Chun-Shing Lee<sup>6,2</sup>, Hai-Yao Deng<sup>7</sup>, Feng Wang<sup>8</sup>, Yilong Han<sup>8</sup>, Cho-Tung Yip<sup>6,†</sup> and Chi-Hang Lam<sup>2,‡</sup>

<sup>1</sup>*Department of Computer Science, University of Warwick, Coventry, UK*

<sup>2</sup>*Department of Applied Physics, Hong Kong Polytechnic University, Hong Kong, China*

<sup>3</sup>*Department of Physics, Yale University, New Haven, Connecticut 06511, USA.*

<sup>4</sup>*Department of Physics, North Carolina State University, Raleigh, NC 27695, USA*

<sup>5</sup>*School of Mathematics and Physics, Hebei University of Engineering, Handan City 056038, China*

<sup>6</sup>*Department of Physics, Harbin Institute of Technology, Shenzhen 518055, China*

<sup>7</sup>*School of Physics and Astronomy, Cardiff University, 5 The Parade, Cardiff CF24 3AA, Wales, UK*

<sup>8</sup>*Department of Physics, Hong Kong University of Science and Technology, Clear Water Bay, Hong Kong, China*

The nature of glassy dynamics and the glass transition are long-standing problems under active debate. In the presence of a structural disorder widely believed to be an essential characteristic of structural glass, identifying and understanding key dynamical behaviors are very challenging. In this work, we demonstrate that an energetic disorder, which usually results from a structural disorder, is instead a more essential feature of glass. Specifically, we develop a distinguishable-particle glassy crystal (DPGC) in which particles are ordered in a face-centered cubic lattice and follow particle-dependent random interactions, leading to an energetic disorder in the particle configuration space. Molecular dynamics simulations in the presence of vacancy-induced particle diffusion show typical glassy behaviors. A unique feature of this molecular model is the knowledge of the complete set of inherent structures with easily calculable free energies, implying a well-understood potential energy landscape. Due to its simplicity, the study of the DPGC provides a promising direction to unlock the mysteries of glass.

There are many open questions regarding the dynamics of structural glass and the nature of the glass transition despite decades of intensive study [1–4]. Glass formers constitute an immensely diverse group of materials. Besides many fascinating phenomena in the bulk, they also exhibit puzzling features in confined geometries [5, 6]. A typical glass is characterized by a structural disorder with random and frustrated particle positions and, for non-spherical molecules, also orientations. A type of glass, called orientational glassy crystal, possesses a crystalline structure but has random molecular orientations which constitute a structural disorder [7]. In view of the wide range of materials and physical conditions, identifying and understanding the most fundamental features of glass have proven very challenging.

In general, the structural disorder of glass amounts to momentarily quenched random particle separations and (or) orientations. This implies random particle interactions and hence also an energetic disorder. An important question is whether structural disorder plays other crucial roles in glassy dynamics apart from generating the energetic disorder. By studying a distinguishable-particle glassy crystal (DPGC), we show that structural disorder plays no other role in many glassy properties. The DPGC is a molecular model of glass with an energetic disorder, but it is structurally ordered with neither positional nor orientational disorder. The DPGC is in our knowledge the simplest molecular model of glass. It is characterized

by vacancy-induced dynamics. The inherent structures are trivially known. It is also the only known molecular model with solvable equilibrium statistics. It can be an ideal example for studying glassy dynamics.

The model is a direct molecular generalization of the distinguishable-particle lattice model (DPLM), which has successfully reproduced many glassy phenomena [8–15] including non-trivial ones such as Kovacs paradox [10], a wide range of fragilities [11], and diffusion coefficient power-laws upon partial swap [12]. The energetics in the DPLM is dictated by particle-dependent nearest neighbor pair interactions and the kinetics is characterized by void-induced particle hops [11]. It requires no explicit kinetic or energetic constraint [16–18], enabling a generalization to a molecular model.

We consider dynamics dominated by vacancy-induced particle hops. Voids, the counterpart of vacancy in glass, or related defects have long been suggested to be responsible for glassy dynamics [19–22]. Recently, quasivoids, i.e. voids in a fragmented form, have been identified to dominate dynamics in glassy colloidal experiments [23] and this justifies the use of vacancy-induced dynamics in this work.

## I. MODEL

In the DPGC,  $N$  distinguishable particles form a face-centered cubic (FCC) lattice in 3D (see yellow region in Fig. 1). The interaction energy  $\Phi_{kl}(r)$  between particles  $k$  and  $l$  separated by a distance  $r$  follows the Lennard-

\* These authors contributed equally

† Email: h0260416@gmail.com

‡ Email: C.H.Lam@polyu.edu.hk

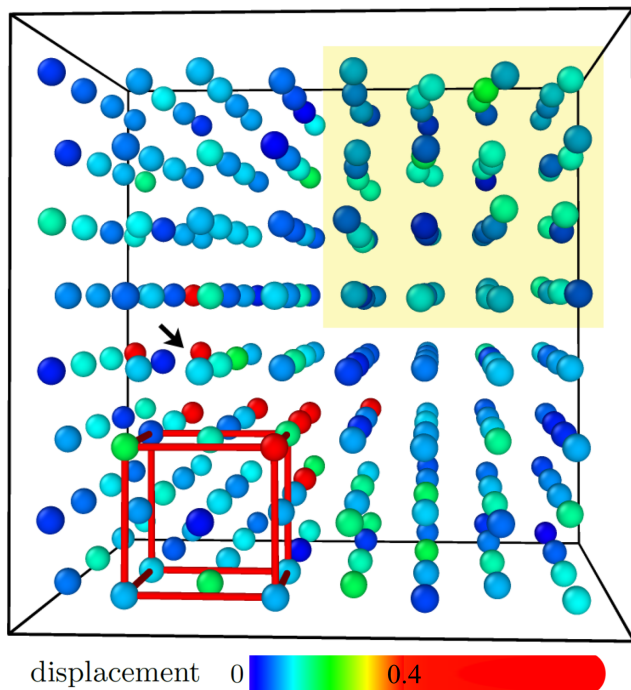


Figure 1. A snapshot of a small-scale DPGC with 255 particles and one vacancy (black arrow) following an FCC structure in a cubic simulation box at  $T = 0.3$ . Particle colors indicate displacements from 0 to  $0.4\sigma$  over a duration of  $2 \times 10^5$ . Particles with displacements beyond  $0.4\sigma$  (red) have hopped at least once. The majority of particle movement is found near the vacancy. Particles at the top right corner (yellow region) are shown at their instantaneous positions. Other particles are shown at their inherent structural positions. A small red cube represents the FCC unit cell.

Jones (LJ) potential:

$$\Phi_{kl}(r) = -4V_{kl} \left[ \left( \frac{\sigma}{r} \right)^{12} - \left( \frac{\sigma}{r} \right)^6 \right] \quad (1)$$

with a distance cut off of  $2.5\sigma$  beyond which it becomes a constant with respect to  $r$ . We fix  $\sigma = 1$  which defines the length scale in our system. Each  $V_{kl} < 0$  represents a particle-dependent energy depth of the LJ potential and is a quenched random variable following a uniform distribution  $g(V)$  in the range  $[-1, -0.25]$  [24]. The random depth  $V_{kl}$  is analogous to random interactions in the DPLM which follows a range  $[-0.5, 0.5]$  designed to minimize effective vacancy-vacancy attraction [11]. This range is not appropriate for the DPGC as  $V_{kl}$  must now be negative. To avoid vacancy aggregation, we instead have to employ a small vacancy density.

Our main molecular dynamics (MD) simulations are performed in the NVT ensemble in a cubic box with  $13^3$  FCC unit cells under periodic boundary conditions. The lattice points are occupied by  $N = 8780$  particles with  $N_v = 8$  vacancies, corresponding to a vacancy density of  $\phi_v \simeq 0.091\%$  per lattice point. The lattice constant is set at  $a_0 = 1.6\sigma$ . This implies a nearest-neighbor distance of

$a_0/\sqrt{2} \simeq 1.131\sigma$  and a small tensile strain which has been found necessary to break a form of divacancy-particle complex. The FCC structure is remarkably stable below the melting temperature of about 0.83. In contrast, a disordered form of the system is stable only if a bimodal distribution of particle diameters is adopted [25]. The DPGC can be brought to equilibrium using swap and a ghost particle method (see appendix).

## II. GLASSY CHARACTERISTICS

We now explain standard measurements on our MD simulations of the DPGC demonstrating glassy behaviors. First, an energy hysteresis is observed during a cooling/heating cycle. Starting from an equilibrium system at temperature 0.7, it is cooled to 0.2 and then heated back to 0.7 at the same cooling/heating rate  $\nu$ . Figure 2 plots the average potential energy per particle  $E/N$  against temperature  $T$  for two values of  $\nu$ . We observe a clear energy hysteresis with kinks signifying glass transitions. The glass transition temperature  $T_g$  can be found from the intersection of the two relatively linear sections of the heating curves [26]. We get  $T_g \simeq 0.41$  and  $0.44$  for  $\nu = 5 \times 10^{-7}$  and  $10^{-6}$  respectively, showing that  $T_g$  increases with  $\nu$  as expected of glass.

The glass transition temperature  $T_g$  separates two phases of the system exhibiting different dynamics. Below  $T_g$ , the system enters the glass phase with largely frozen particle allocations to the lattice points. Particle motions are mainly vibrations and back-and-forth hops. Above  $T_g$ , particles perform vacancy-induced hops around various lattice positions within practical observation times. This rearranges the particles in the lattice and relaxes the pair interactions. We propose to call it the dynamic phase, which is analogous to the liquid phase of conventional glass formers. Importantly, such energy relaxation in the dynamic phase, akin to glassy materials, is absent in monoatomic crystals.

Recognizing that in the glass phase, particles hop infrequently, we measure  $T_g$  based on particle mean square displacement (MSD), which provides better statistics. When cooling the system from 0.7 to a low temperature  $T_0 = 0.2$  at a rate  $\nu$ , we measure the MSD from the particle position  $\mathbf{r}(T)$  at temperature  $T$  to the final frozen position  $\mathbf{r}(T_0)$ , i.e.  $\text{MSD} = \langle |\mathbf{r}(T) - \mathbf{r}(T_0)|^2 \rangle$ . We define  $T_g$  as the temperature at which on average, all particles have hopped away from their initial positions once, to a neighboring lattice point before becoming frozen, i.e.  $\text{MSD} = a_0^2/2$ . Figure 3(a) plots  $\nu$  against the measured  $1/T_g$ . The linearity in the semi-log plot shows  $\log(\nu) \sim 1/T_g$ , consistent with typical glassy characteristics [26]. In particular, it indicates that the present DPGC is a strong glass.

Concerning equilibrium properties, we have measured the self-intermediate scattering function (SISF) from which the structural relaxation time  $\tau$  and the stretching exponent  $\beta$  are obtained. Figure 3(b) show  $\tau$  against

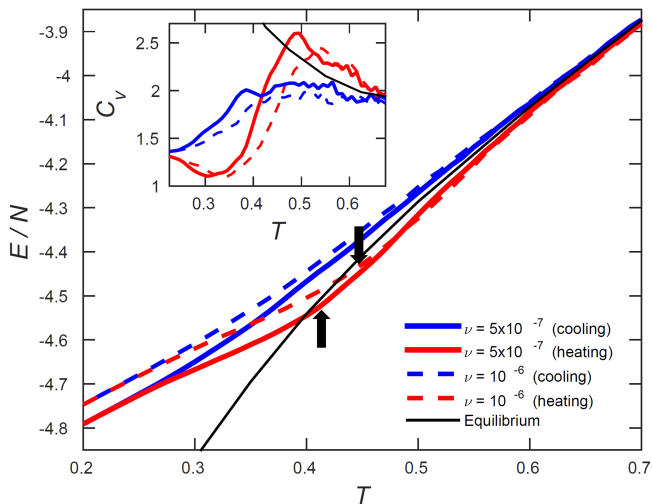


Figure 2. Potential energy per particle  $E/N$  against temperature  $T$  during cooling (blue) and heating (red) with rates  $\nu = 5 \times 10^{-7}$  and  $10^{-6}$ . The black line shows the equilibrium energy. Black arrows shows  $T_g$  for both rates. Inset shows heat capacity  $C_v$  against  $T$ .

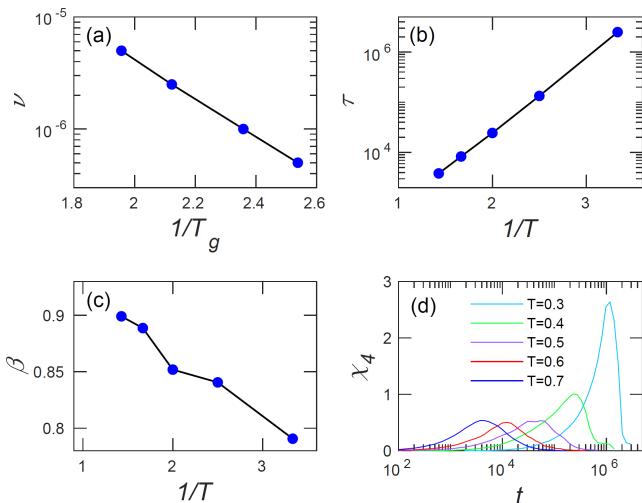


Figure 3. Characterization of glassy properties from cooling (a) and equilibrium (b)-(d) simulations. (a) A semi-log plot of  $\nu$  against  $1/T_g$  based on MSD measurements. (b) Structural relaxation time  $\tau$  and (c) Stretching exponent  $\beta$  against  $1/T$  extracted from the self-intermediate scatter function. (d) Four-point susceptibility  $\chi_4(t)$  against time  $t$ .

$1/T$ . A linear behavior in the semi-log plot again indicates a strong glass. The stretching exponent  $\beta$  shown in Fig. 3(c) is less than 1 and decreases with  $1/T$ . We have also computed the four-point correlation function  $\chi_4$  as plotted in Fig. 3(d). It shows a peak which grows in height as  $T$  decreases, a typical feature indicating a growing dynamic heterogeneity.

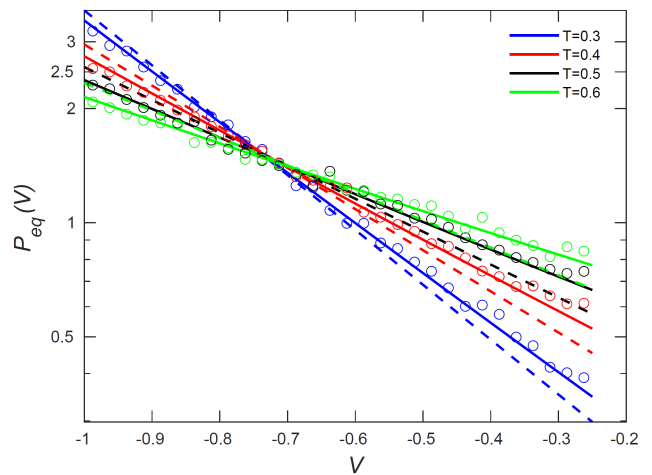


Figure 4. Equilibrium distribution  $P_{eq}(V)$  of pair interaction energy depth  $V$  between neighbor particles from simulations (symbols). Dashed lines are theoretical predictions in Equation (5) and solid lines are from Eqs. (3) and (4).

### III. INHERENT STRUCTURE

Glassy dynamics can be formulated in terms of transitions among inherent structures, which are meta-stable states of the system [27]. Performing an energy minimization numerically, the DPGC arrives always at an inherent structure which is simply a FCC lattice of a certain particle and vacancy arrangement with vibrations suppressed, as shown in Fig. 1. The system is brought to equilibrium using swap and a ghost particle method (see appendix). The number of possible inherent structures is  $(N + N_v)!/N_v!$ , noting the  $N$  distinguishable particles and  $N_v$  identical vacancies.

The free energy  $F_{IS}$  of an inherent structure can be expressed as  $F_{IS} = -k_B T \ln P_{IS}$ , where  $P_{IS}$  is its occurrence probability. Analogous to exact equilibrium statistics of the DPLM [8, 11], we propose that  $P_{IS}$  can be approximately factorized over the interactions and is given by

$$P_{IS} = \prod_{kl} P_{eq}(V_{kl}), \quad (2)$$

where the product is over all nearest neighboring particles  $k$  and  $l$ . Here,  $P_{eq}(V)$  is the equilibrium probability of a pair interaction given by (see also section below)

$$P_{eq}(V) = \frac{1}{\mathcal{N}} e^{-V/k_B T} g(V) \Psi(V) \quad (3)$$

where  $\Psi(V)$  accounts for energetic and entropic effects of vibrations and can be approximated as

$$\Psi(V) = (-V - 3\bar{V}/2)^{-\frac{1}{2}} \quad (4)$$

with  $\bar{V}$  being the mean value of  $V$  and  $\mathcal{N}$  following from the normalization  $\int P_{eq}(V) dV = 1$ . For the DPLM without vibration,  $\Psi(V) \equiv 1$  and Equation (3) is exact

[8, 10, 11]. For the DPGC, we have measured  $P_{eq}(V)$  based on the inherent structures from equilibrium simulations. Results are plotted in Fig. 4 showing a good agreement with Eqs. (3) and (4).

#### IV. EQUILIBRIUM STATISTICS

Approximate equilibrium statistics of the DPGC can be calculated by generalizing an exact method used for the DPLM. Specifically, we study the equilibrium distribution  $P_{eq}(V)$  of the energy depth  $V$  of the pair interactions realized between neighboring particles. Measured values of  $P_{eq}(V)$  are shown in Figure 4 in semi-log scales.

A rough estimate  $P_{eq}^0(V)$  of  $P_{eq}(V)$ , assuming naively a simple Boltzmann weight  $e^{-V/k_B T}$  following DPLM results, is given by

$$P_{eq}^0(V) \propto e^{-V/k_B T} g(V). \quad (5)$$

Equation (5) has been proven exact for the DPLM when  $V$  is taken as the pair interaction. Figure 4 compares  $P_{eq}^0(V)$  with the numerically measured  $P_{eq}(V)$  and shows a fair agreement.

We note that the DPGC differs from the DPLM mainly by having particle vibrations. Generalizing Equation (5) to account for energetic and entropic effects of vibrations approximately, we replace the Boltzmann factor in Equation (5) by the partition function  $Z_1(V)$  of an interaction of depth  $V$  as follows

$$P_{eq}(V) \propto Z_1(V)g(V), \quad (6)$$

where

$$Z_1(V) = \int_0^\infty \exp[-E_V(r)] dr \quad (7)$$

with  $E_V(r)$  being the average system energy when an interaction of depth  $V$  is at bond length  $r$ . More precisely, we focus on the interaction between neighboring particles  $k$  and  $l$  of depth  $V$  separated by a distance  $r$ . Assume for simplicity that only particles  $k$  and  $l$  vibrate in the breathing, i.e. symmetric, mode and all other particles are stationary at the lattice positions. The separation can be expressed in terms of particle displacement  $s$  as  $r = r_0 + 2s$  with  $r_0 = 2^{1/6}\sigma$ . Assume that all other interactions have a uniform depth  $\bar{V}$  given by its average value

$$\bar{V} = \int V P_{eq}^0(V) dV. \quad (8)$$

An analysis of the 23 interactions among particles  $k$  and  $l$  and nearest neighbors in the FCC lattice indicates that only 11 interactions depend on  $s$  up to the linear order and we get

$$E_V(s) = \Phi(V, 2s) + 2\Phi(\bar{V}, -s) + 4\Phi(\bar{V}, s/\sqrt{2}) + 4\Phi(\bar{V}, -s/\sqrt{2}), \quad (9)$$

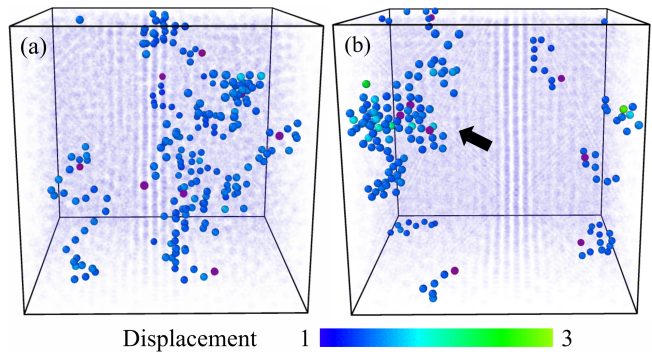


Figure 5. Particles with large displacements from 1 (blue) to 3 (green) at  $T=0.7$  (a) and  $0.25$  (b). Displacements are measured over a duration at which the particle MSD equals  $0.1\sigma$ . Purple spheres represent vacancies. A black arrow in (b) indicates a region with a strong facilitation among vacancies.

where the Lennard-Jones potential is parametrized as

$$\Phi(V, s) = -4V \left[ \left( \frac{\sigma}{r_0 + 2s} \right)^{12} - \left( \frac{\sigma}{r_0 + 2s} \right)^6 \right]. \quad (10)$$

For further simplicity, we use a harmonic approximation for the LJ potential, i.e.

$$\Phi(V, s) = -\frac{1}{2}KV \cdot (2s)^2 + V, \quad (11)$$

where  $K$  is an effective elastic constant. Equation (7) then involves a simple Gaussian integral which can be evaluated to get

$$Z_1(V) = \exp\left(-\frac{V + 10\bar{V}}{k_B T}\right) \sqrt{-\frac{4\pi k_B T}{2KV + 3K\bar{V}}}. \quad (12)$$

Using also Equation (6), we have

$$P_{eq}(V) = \frac{1}{\mathcal{N}} e^{-V/k_B T} g(V) \left(-V - \frac{3}{2}\bar{V}\right)^{-\frac{1}{2}}, \quad (13)$$

where factors independent of  $V$ , such as  $K^{-1/2}$ , have been rescaled away when defining the normalization constant  $\mathcal{N}$ . Equation (13) agrees well with simulation results as shown in Figure 4.

The success of Equation (13) in describing our simulations show that interactions in a system is approximately independent of each other, which is an exact result for the DPLM. As a consistency check, at a very low  $T$ ,  $P_{eq}(V)$  is non-negligible only for  $V \simeq \bar{V}$  so that the last factor in Equation (13) approaches a constant. Then,  $P_{eq}(V)$  converges to  $P_{eq}^0(V)$  as vibrations diminish.

#### V. DYNAMICAL HETEROGENEITY

The DPGC exhibits dynamical heterogeneity as indicated by a growing  $\chi_4$  at decreasing  $T$  shown in Fig. 3(d).

This is however easy to understand in general for systems following defect-induced dynamics including glassy or simple crystals with vacancies as well as partial-swap systems [12]. The idea can also apply to conventional glasses if one assumes quasivoid-induced dynamics [23]. To illustrate the heterogeneity in real space, Fig. 5 highlights particles in the DPGC with large displacements. As seen, they concentrate close to the vacancies. The vacancy-induced nature of particle hops immediately explains the dynamic heterogeneity. It also explains the observed stringlike geometries of the set of hopping particles [28, 29], revealing the paths taken by the vacancies. Note that vacancy-induced motion realizes a defect-particle facilitation process [8, 22, 30, 31], which also mediates facilitation among particles [32, 33].

At  $T = 0.7$  [Fig. 5(a)], various vacancies have rather similar mobilities. As  $T$  decreases to 0.25 [Fig. 5(b)], isolated vacancies are observed to slow down more significantly, and mobility is dominated by groups of vacancies. Specifically, when vacancies are energetically attracted to each other, adjacent particles become loosely bonded and hop more rapidly, speeding up locally the motions of both the particles and the vacancies. This realizes a form of defect-defect facilitation mainly of an energetic origin. Particles close to groups of vacancies thus enjoy enhanced dynamics and this increases the dynamic heterogeneity at low  $T$ . Nevertheless, such facilitation is distinct from facilitation of a dynamic origin in the absence of defect attraction [22, 30, 31] as has been observed in the DPLM [8, 34]. Further work is ongoing to control the vacancy-vacancy attraction based on alternative particle potentials so as to implement facilitation better resembling that in conventional glasses.

## VI. RELAXATION TIME

We measure the self-intermediate scattering function defined as

$$F_s(q, t) = \left\langle e^{i\mathbf{q} \cdot (\mathbf{r}_l(t) - \mathbf{r}_l(0))} \right\rangle, \quad (14)$$

where  $|\mathbf{q}| = 2\pi/\lambda$  with  $\lambda = a_0/\sqrt{2}$  being the nearest neighbor distance. Results are plotted in Fig. 6(a) showing a two-step relaxation. The second terminal decay is well approximated by the Kohlrausch-Williams-Watts (KWW) stretched exponential function of the form  $A \exp[-(t/\tau)^\beta]$ , where  $\tau$  is the structural relaxation time,  $\beta$  ( $0 < \beta < 1$ ) is the stretching exponent and  $A \simeq 1$ . Our results fit well to the KWW form as demonstrated by a linear region at large  $t$  in the log-log plot of  $-\log(F_s(q, t))$  against  $t$  in Fig. 6(b). The fitted values of  $\tau$  and  $\beta$  are plotted in Figure 3(b)-(c).

## VII. DIFFUSION COEFFICIENT

We calculate the particle mean-squared displacement (MSD) defined as  $\langle |\mathbf{r}_l(t) - \mathbf{r}_l(0)|^2 \rangle$  where  $\mathbf{r}_l(t)$  denotes

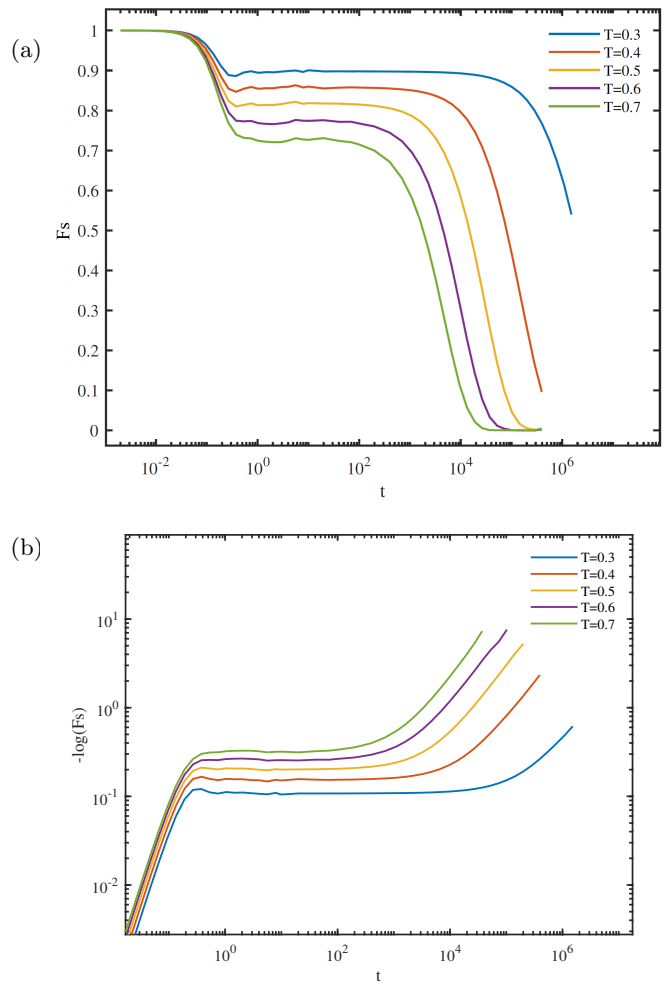


Figure 6. Self-intermediate scattering function  $F_s(q, t)$  against  $t$  in a semi-log plot (a) and  $-\log(F_s(q, t))$  against  $t$  in a log-log plot (b) using the same set of data.

the position of particle  $l$  at time  $t$ . Figure 7 shows the MSD in a log-log plot for different temperature  $T$ . At long time in the diffusive regime with the MSD is beyond  $\sigma$ , we measure the particle diffusion coefficient from

$$D = \frac{1}{2d} \frac{MSD}{t} \quad (15)$$

where  $d = 3$  indicates three-dimensional space. Results are shown in Fig. 8.

Figure 9 plots  $D\tau$  against  $1/T$ . We observe that  $D\tau$  increases with decreasing  $T$ , demonstrating a violation of the Stokes-Einstein relation as expected for glasses. The violation is nevertheless slight as we cannot reach deeper supercooling due to computational limitations.

## VIII. FOUR-POINT CORRELATION

Dynamic heterogeneity is the behavior in glass formers that some regions relax much faster than the others. To quantitatively study dynamic heterogeneity, one first

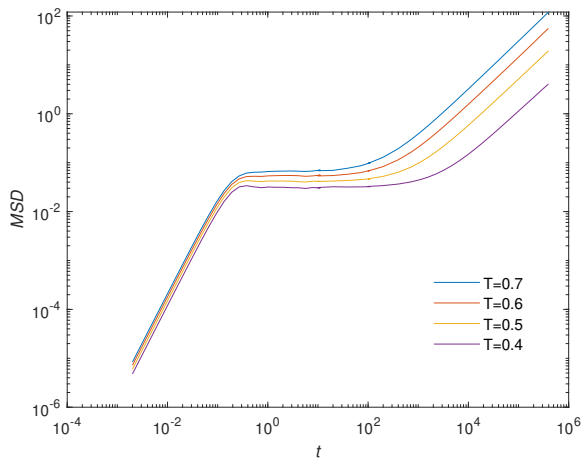
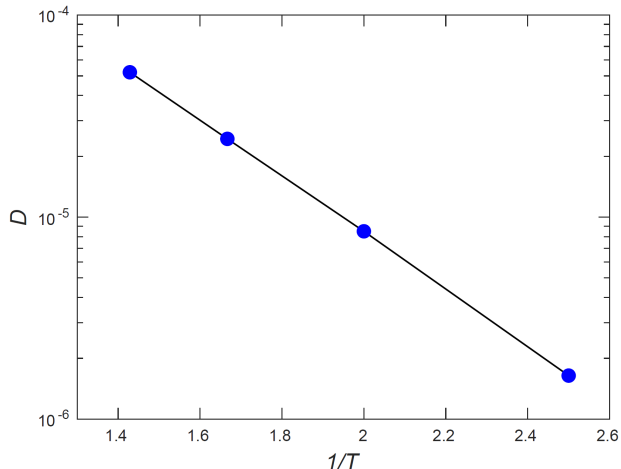


Figure 7. MSD in log-log plot against time.

Figure 8. Semi-log plot of  $D$ , showing the Arrhenius relation.

defines an overlap function as

$$c_l(t, 0) = e^{i\mathbf{q} \cdot (\mathbf{r}_l(t) - \mathbf{r}_l(0))}. \quad (16)$$

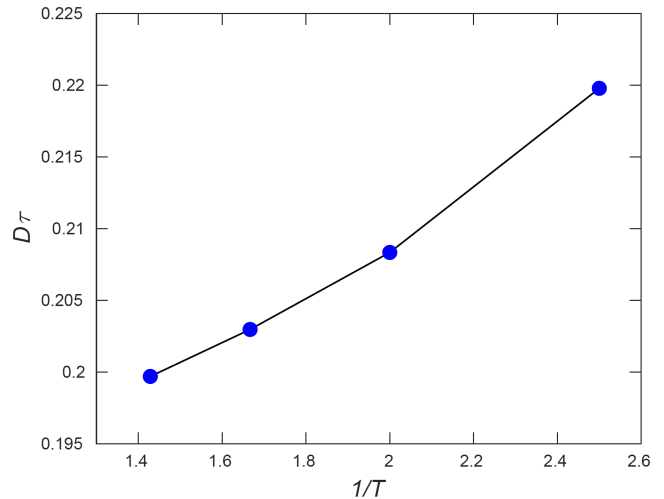
where  $|\mathbf{q}| = 2\pi/\lambda$  with  $\lambda = a_0/\sqrt{2}$ . Note that the average overlap equals the self-intermediate scattering function  $F_s(q, t)$ . Each particle contributes to an overlap field defined by

$$c(\mathbf{r}; t, 0) = \sum_l c_l(t, 0) \delta(\mathbf{r} - \mathbf{r}_l(0)), \quad (17)$$

where the sum is over all particles  $l$ . Consider its spatial correlation

$$G_4(\mathbf{r}, t) = \langle c(\mathbf{r}; t, 0)c(\mathbf{0}; t, 0) \rangle - \langle c(\mathbf{0}; t, 0) \rangle^2 \quad (18)$$

where the average is over the spatial origin  $\mathbf{0}$  and the starting time 0. Then,  $G_4$  measures the correlation of the fluctuations in the overlap function between two points

Figure 9. Plot of  $D\tau$  against  $1/T$ . A non-constant value indicates a violation of the Stokes-Einstein relation.

that are separated by  $\mathbf{r}$ . In the Fourier space, we get

$$\begin{aligned} S_4(\tilde{\mathbf{q}}, t) &= \int e^{i\tilde{\mathbf{q}} \cdot \mathbf{r}} G_4(\mathbf{r}, t) d\mathbf{r} \quad (19) \\ &= N \left\langle \left| \frac{1}{N} \sum_l e^{i\tilde{\mathbf{q}} \cdot \mathbf{r}_l(0)} (c_l(t, 0) - F_s(q, t)) \right|^2 \right\rangle \quad (20) \end{aligned}$$

We then define the susceptibility as  $\chi_4(t) = \lim_{\tilde{q} \rightarrow 0} S_4(\tilde{\mathbf{q}}, t)$ , which is simply the variance of the overlap function. One can interpret  $\chi_4(t)$  as the typical size of correlated clusters in structural relaxation and it is thus a measure of the degree of dynamic heterogeneity.

Figure 3(d) shows  $\chi_4(t)$  measured from the simulations. As is typical for structural glass,  $\chi_4(t)$  has a peak for each temperature, which shifts to larger times and has a larger height when  $T$  decreases. This reveals an increasing length scale of dynamic heterogeneity when the system cools down.

## IX. RETURNING AND ESCAPING HOPS

As temperature decreases, dynamics slows down not only because of the reduced particle hopping rate but also an increased back-and-forth tendency of the hopping motions due to the rugged potential energy landscape. We now quantify this anti-correlation in successive hops of a particle. Specifically, after a particle has hopped, we measure the probability  $P_{ret}$  that its next hop returns itself to the original lattice point. The probability  $P_{esc}$  that it hops next instead to a new lattice position is also measured. Figure 10 shows the results. At a high  $T = 0.7$ , we find that  $P_{ret} \simeq 0.095$ , which is close to 0.0833 for an uncorrelated random walk on the FCC lattice. As  $T$  decreases,  $P_{ret}$  increases monotonically and reaches 0.33

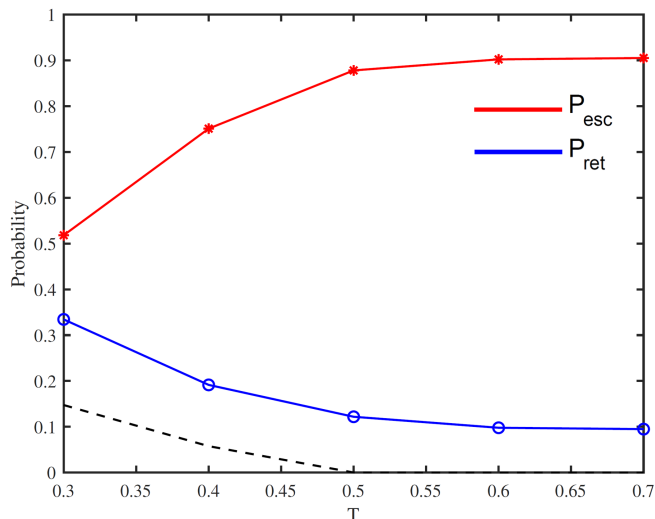


Figure 10. Probabilities  $P_{ret}$  and  $P_{esc}$  for returning and escaping second hops of particles after previous hopping events against temperature  $T$ . The black dashed line indicates the probability that no second hop occurs during the observation period.

for the lowest  $T = 0.3$  studied. This shows a strong anti-correlation in the hopping events, revealing the impact of the rugged potential energy landscape due to the random pair interactions.

## X. MELTING

Figure 2 shows an energy hysteresis during a cooling and heating cycle. Here, we extend the heating process to a higher temperature as shown in Fig. 11 for a cooling/heating rate  $\nu = 10^{-6}$ . At  $T \simeq 0.83$ , an abrupt jump of the energy indicates the melting of the FCC lattice, as the system becomes structurally disorder after the transition. All other simulations in this work are performed well below 0.83 so that the FCC lattice is stable.

## XI. DISCUSSIONS

The DPGC possesses no structural disorder. It implements directly an energetic disorder via random interactions which usually results instead from a structure disorder. Its ability to exhibit glassy properties suggests that energetic disorder may play a more direct and essential role than structural disorder in glassy dynamics. Studying structurally ordered glasses, like the DPGC, can be a much simpler step to understand glass. Note that spin glass [35, 36] also directly assumes an energetic disorder, which however is quenched in the real space. Instead, the disorder in the DPGC and the DPLM is quenched only in the configuration space [8], making it appropriate for structural glass.

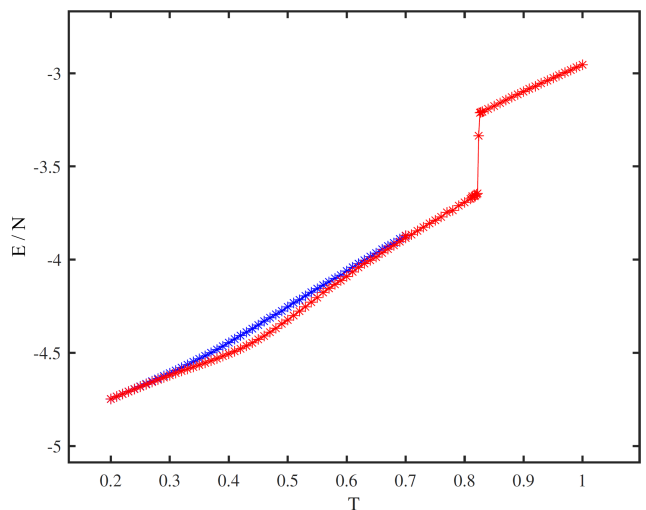


Figure 11. Potential energy per particle  $E/N$  against temperature  $T$  during cooling (blue) and heating (red) with a rate  $\nu = 10^{-6}$ . The abrupt jump at  $T \simeq 0.83$  signifies melting of the FCC lattice.

Being a straightforward molecular generalization of the DPLM, properties reported here for the DPGC in general are inherited from and are closely analogous to those of the DPLM, except those related to lattice vibrations. The realization of the DPGC strongly supports the physical relevance of the DPLM. Conversely, we expect that glassy phenomena already demonstrated by the DPLM [8–15] likely apply also to the DPGC. These features of the DPLM support the idea that the DPGC describes a typical glass rather than a new type of glass.

Our system exhibits three phases. As  $T$  increases from below  $T_g$ , it crosses over from the glass phase, in which particles hardly hop within practical observation times, to the dynamic phase, in which the system readily relaxes via particle rearrangements among the lattice positions. The static structures of both phases follow the same FCC lattice. At higher  $T$ , it melts into the liquid phase. The glass and dynamic phases of the DPGC separated by a glass transition generalize the glass and supercooled-liquid phases of conventional glass formers.

The complete set of inherent structures [27] is known with the occurrence probabilities  $P_{IS}$  and free energy  $F_{IS}$  given in Eqs. (2)-(4). This is, in our knowledge, unique in all molecular glassy systems, including orientational glassy crystals [7]. Furthermore, the known  $F_{IS}$  also directly implies a full knowledge of the potential energy landscape (PEL) [37] expressible as a function of inherent structures. It is a rugged PEL due to random pair interactions, in sharp contrast to simple crystals and assumptions in early defect theories [19].

The elementary motions in the relaxation of the DPGC are vacancy-induced particle hops. This is analogous to deeply supercooled liquids in which quasivoids-induced particle hops may dominate [23]. With the full knowledge of the PEL, a transition state theory of the dynamics

[38] can be straightforwardly formulated. For example, with  $N_v$  monovacancies, an inherent structure is directly connected by possible transitions to  $12N_v$  others, noting that there are 12 possible hopping directions of each vacancy. In the context of the DPLM, such an analysis implies that the energetically favorable domain of the PEL takes a random-tree geometry in the configuration space, leading to emergent kinetic constraints and facilitation [34, 39]. Implications to the DPGC will be studied in the future.

An accurate experimental realization of the DPGC may be challenging. One complication concerns the random particle-dependent interactions in which interaction depth between particles  $k$  and  $l$  is uncorrelated to that between particles  $k$  and  $l'$ . However, allowing for correlations among the interactions, a 2D lattice of polydispersed colloidal particle system has shown signs of glassy

properties [40]. Alternatively, limiting to few particle types, our system is analogous to high-entropy alloys [41]. The DPGC can serve as an idealized model for studying various types of glass.

In conclusion, we have developed a distinguishable-particle glassy crystal model which shows typical glassy behaviors. The inherent structures are known and numerable with their approximate equilibrium probabilities available analytically. This makes it, in our opinion, the simplest molecular model of glass. It also demonstrates that a structural disorder is not essential in the presence of an energetic disorder to exhibit glassy properties.

We are grateful to Giorgio Parisi and Paolo Balden for helpful discussions. This work was supported by General Research Fund of Hong Kong (Grant 15303220), National Natural Science Foundation of China (Grant No. 1217040938, 12174079 and 11974297).

- 
- [1] F. H. Stillinger and P. G. Debenedetti, Glass transition thermodynamics and kinetics, *Annu. Rev. Condens. Matter Phys.* **4**, 263 (2013).
- [2] G. Biroli and J. P. Garrahan, Perspective: The glass transition, *J. Chem. Phys.* **138**, 12A301 (2013).
- [3] G. B. McKenna and S. L. Simon, 50th anniversary perspective: Challenges in the dynamics and kinetics of glass-forming polymers, *Macromolecules* **50**, 6333 (2017).
- [4] F. Arceri, F. P. Landes, L. Berthier, and G. Biroli, Glasses and aging, a statistical mechanics perspective on, in *Statistical and Nonlinear Physics* (Springer, 2022) p. 229.
- [5] F. Chen, C.-H. Lam, and O. K. C. Tsui, The surface mobility of glasses, *Science* **343**, 975 (2014).
- [6] C. B. Roth, Polymers under nanoconfinement: where are we now in understanding local property changes?, *Chemical Society Reviews* **50**, 8050 (2021).
- [7] U. T. Höchli, K. Knorr, and A. Loidl, Orientational glasses, *Adv. Phys.* **39**, 405 (1990).
- [8] L.-H. Zhang and C.-H. Lam, Emergent facilitation behavior in a distinguishable-particle lattice model of glass, *Phys. Rev. B* **95**, 184202 (2017).
- [9] C.-S. Lee, H.-Y. Deng, C.-T. Yip, and C.-H. Lam, Large heat-capacity jump in cooling-heating of fragile glass from kinetic monte carlo simulations based on a two-state picture, *Phys. Rev. E* **104**, 024131 (2021).
- [10] M. Lulli, C.-S. Lee, H.-Y. Deng, C.-T. Yip, and C.-H. Lam, Spatial heterogeneities in structural temperature cause kovacs' expansion gap paradox in aging of glasses, *Phys. Rev. Lett.* **124**, 095501 (2020).
- [11] C.-S. Lee, M. Lulli, L.-H. Zhang, H.-Y. Deng, and C.-H. Lam, Fragile glasses associated with a dramatic drop of entropy under supercooling, *Phys. Rev. Lett.* **125**, 265703 (2020).
- [12] G. Gopinath, C.-S. Lee, X.-Y. Gao, X.-D. An, C.-H. Chan, C.-T. Yip, H.-Y. Deng, and C.-H. Lam, Diffusion-coefficient power laws and defect-driven glassy dynamics in swap acceleration, *Phys. Rev. Lett.* **129**, 168002 (2022).
- [13] M. Lulli, C.-S. Lee, L.-H. Zhang, H.-Y. Deng, and C.-H. Lam, Kovacs effect in glass with material memory revealed in non-equilibrium particle interactions, **2021**, 093303 (2021).
- [14] X.-Y. Gao, H.-Y. Deng, C.-S. Lee, J. You, and C.-H. Lam, Emergence of two-level systems in glass formers: a kinetic monte carlo study, *Soft Matter* **18**, 2211 (2022).
- [15] X.-Y. Gao, C.-Y. Ong, C.-S. Lee, C.-T. Yip, H.-Y. Deng, and C.-H. Lam, Kauzmann paradox: A possible crossover due to diminishing local excitations, *Phys. Rev. B* **107**, 174206 (2023).
- [16] J. P. Garrahan, P. Sollich, and C. Toninelli, Kinetically constrained models, in *Dynamical Heterogeneities in Glasses, Colloids and Granular Media*, edited by L. Berthier, G. Biroli, J.-P. Bouchaud, L. Cipelletti, and W. van Saarloosand (Oxford University Press, 2011).
- [17] F. Ritort and P. Sollich, Glassy dynamics of kinetically constrained models, *Adv. Phys.* **52**, 219 (2003).
- [18] G. Biroli and M. Mézard, Lattice glass models, *Phys. Rev. Lett.* **88**, 025501 (2001).
- [19] S. H. Glarum, Dielectric relaxation of isoamyl bromide, *J. Chem. Phys.* **33**, 639 (1960).
- [20] G. H. Fredrickson and S. A. Brawer, Monte carlo investigation of a kinetic ising model of the glass transition, *J. Chem. Phys.* **84**, 3351 (1986).
- [21] S. Napolitano and D. Cangialosi, Interfacial free volume and vitrification: reduction in  $t_g$  in proximity of an adsorbing interface explained by the free volume holes diffusion model, *Macromolecules* **46**, 8051 (2013).
- [22] C.-H. Lam, Repetition and pair-interaction of string-like hopping motions in glassy polymers, *J. Chem. Phys.* **146**, 244906 (2017).
- [23] C.-T. Yip, M. Isobe, C.-H. Chan, S. Ren, K.-P. Wong, Q. Huo, C.-S. Lee, Y.-H. Tsang, Y. Han, and C.-H. Lam, Direct evidence of void-induced structural relaxations in colloidal glass formers, *Phys. Rev. Lett.* **125**, 258001 (2020).
- [24] L. S. Shagolsem, D. Osmanović, O. Peleg, and Y. Rabin, Communication: Pair interaction ordering in fluids with random interactions, *J. Chem. Phys.* **142**, 051104 (2015).
- [25] H. Qin, C.-S. Lee, C.-H. Lam, and Y. Lü, Decoupling limit of diffusion and structural relaxation predicted by a fragility-tunable glassy model, *Phys. Rev. B* **108**, 104105

- (2023).
- [26] I. M. Hodge, Enthalpy relaxation and recovery in amorphous materials, *J. Non-Cryst. Solids* **169**, 211 (1994).
- [27] F. H. Stillinger and T. A. Weber, Dynamics of structural transitions in liquids, *Phys. Rev. A* **28**, 2408 (1983).
- [28] C. Donati, J. F. Douglas, W. Kob, S. J. Plimpton, P. H. Poole, and S. C. Glotzer, Stringlike cooperative motion in a supercooled liquid, *Phys. Rev. Lett.* **80**, 2338 (1998).
- [29] T. Kawasaki and A. Onuki, Slow relaxations and string-like jump motions in fragile glass-forming liquids: Breakdown of the stokes-einstein relation, *Phys. Rev. E* **87**, 012312 (2013).
- [30] G. H. Fredrickson and H. C. Andersen, Kinetic ising model of the glass transition, *Phys. Rev. Lett.* **53**, 1244 (1984).
- [31] W. Kob and H. C. Andersen, Kinetic lattice-gas model of cage effects in high-density liquids and a test of mode-coupling theory of the ideal-glass transition, *Phys. Rev. E* **48**, 4364 (1993).
- [32] C. K. Mishra, K. H. Nagamanasa, R. Ganapathy, A. K. Sood, and S. Gokhale, Dynamical facilitation governs glassy dynamics in suspensions of colloidal ellipsoids, *Proc. Natl. Acad. Sci.* **111**, 15362 (2014).
- [33] C. Scalliet, B. Guiselin, and L. Berthier, Thirty milliseconds in the life of a supercooled liquid, *Phys. Rev. X* **12**, 041028 (2022).
- [34] C.-H. Lam, Local random configuration-tree theory for string repetition and facilitated dynamics of glass, *J. Stat. Mech.* **2018**, 023301 (2018).
- [35] M. Mézard, G. Parisi, and M.-A. Virasoro, *Spin glass theory and beyond*. (World Scientific, 1990).
- [36] D. Zhou, F. Wang, B. Li, X. Lou, and Y. Han, Glassy spin dynamics in geometrically frustrated buckled colloidal crystals, *Phys. Rev. X* **7**, 021030 (2017).
- [37] F. H. Stillinger, A topographic view of supercooled liquids and glass formation, *Science (New York, N.Y.)* **267**, 1935 (1995).
- [38] M. Vogel, B. Doliwa, A. Heuer, and S. C. Glotzer, Particle rearrangements during transitions between local minima of the potential energy landscape of a binary lennard-jones liquid, *J. Chem. Phys.* **120**, 4404 (2004).
- [39] H.-Y. Deng, C.-S. Lee, M. Lulli, L.-H. Zhang, and C.-H. Lam, Configuration-tree theoretical calculation of the mean-squared displacement of particles in glass formers, *J. Stat. Mech.* **2019**, 094014 (2019).
- [40] C.-H. Chan, Q. Huo, A. Kumar, Y. Shi, H. Hong, Y. Du, S. Ren, K.-P. Wong, and C.-T. Yip, Heterogeneity and memory effect in the sluggish dynamics of vacancy defects in colloidal disordered crystals and their implications to high-entropy alloys, *Advanced Science* **9**, 2205522 (2022).
- [41] J.-W. Yeh, Alloy design strategies and future trends in high-entropy alloys, *JOM* **65**, 1759 (2013).

## Appendix A: Initialization via particle/vacancy swap

System equilibration using standard MD steps can take a very long runtime at low  $T$ . This can be dramatically improved using particle swaps in addition to the MD steps at not too low  $T$ . However, at the lowest  $T = 0.3$  studied, we have found surprisingly that particle swaps fail to equilibrate our system completely. A close examination reveals that even though the distribution of the pair interaction depth  $V$  has already converged to  $P_{eq}(V)$ , the density of di-vacancies is not at equilibrium after particle swaps. This is because the method does not relax the positions of the vacancies. Due to the considerable attraction of the vacancies, the density of di-vacancies should increase as  $T$  decreases but this is not achieved using swaps. For conventional glass models, quasivoids, the counterpart of vacancies, appear unattractive to each other and the problem thus does not apply.

To fully equilibrate the DPGC at  $T = 0.3$ , we have developed a particle/vacancy swap algorithm in addition to the MD steps. For convenience of implementation in LAMMPS, we represent vacancies using *ghost* particles. Specifically, we fill up each vacancy position with a ghost particle, which has a light mass  $m_{ghost} = 0.01$  and a weak interaction depth  $V_{ghost} = -0.01$  with all other particles. Then, they introduce negligible perturbations to the original crystal. A small timestep of 0.0001 is used in the MD steps to avoid the ghost particles being bounced off the system.

The full algorithm for  $T = 0.3$  is as follows. We randomly arrange all real and ghost particles in the FCC lattice. We then perform non-local pairwise particle swaps, irrespective of whether they are real or ghost. This is done as usual by choosing any two particles and swapping their positions with a probability  $\exp(-\Delta E/k_B T)$ , where  $\Delta E$  is the energy change after the swap. The swapping process is performed periodically in between normal MD steps. When equilibrium is attained, as indicated for example by the stabilization of the potential energy, the ghost particles are removed. The system is then further relaxed using conventional swap and MD steps as a safety precaution. We have found that these procedures successfully equilibrate the DPGC at  $T = 0.3$ .